Article

MMS

Mathematics and Mechanics of Solids
2021, Vol. 26(9) 1376–1393

DOI: 10.1177/1081286520984690
journals.sagepub.com/home/mms
SAGE

A new model of bone remodeling and turnover set up in the framework of generalized continuum mechanics

Vittorio Sansalone
MSME, CNRS UMR 8208, Univ Paris Est Creteil, Univ Gustave Eiffel, Creteil, France

Madge Martin
MSME, CNRS UMR 8208, Univ Paris Est Creteil, Univ Gustave Eiffel, Creteil, France; School of Mechanical, Medical and Process Engineering, Queensland University of Technology, Brisbane, Australia

Guillaume Haïat
MSME, CNRS UMR 8208, Univ Paris Est Creteil, Univ Gustave Eiffel, Creteil, France

Peter Pivonka
School of Mechanical, Medical and Process Engineering, Queensland University of Technology, Brisbane, Australia

Thibault Lemaire
MSME, CNRS UMR 8208, Univ Paris Est Creteil, Univ Gustave Eiffel, Creteil, France

Received 23 January 2020; accepted 1 December 2020

Abstract

In the past few decades, numerous studies have attempted to address the various phenomena that take place simultaneously during bone remodeling. Drawing from Frost's "mechanostat theory," multiple phenomenological models of varying complexity have been developed to describe bone remodeling in terms of evolution of bone porosity, tissue properties, and mineralization. The main goal of this paper is to present the general theory of a novel macroscopic and comprehensive model of bone remodeling accounting for the interactions of mechanics and biochemistry at the microscale. Two independent remodeling mechanisms are considered: the rotation of the material axes and the turnover of bone material. The former mechanism is related to the change of orientation of bone microstructure. Bone turnover refers to the dynamic process of bone resorption by osteoclasts, formation of unmineralized bone by osteoblasts, and mineralization. The model is set up in the framework of generalized continuum mechanics. The evolution of bone tissue is thus described through its macroscopic deformation as well as macroscopic variables related to the orientation of bone microstructure and bone tissue composition (porosity, unmineralized and mineralized bone matrix). Thermodynamically consistent evolution laws of bone material are obtained by enforcing suitable statements of the virtual power principle and of the dissipation principle. Moreover, additional constitutive hypotheses are formulated to develop a phenomenological law of bone turnover. The turnover model is discussed on the basis of a number of numerical simulations. Although the

Corresponding author:
Vittorio Sansalone, Laboratoire Modélisation et Simulation Multi Echelle, 61, Avenue du Général de Gaulle, 94010 Créteil Cedex, France.
Email: vittorio.sansalone@u-pec.fr

model can capture the main features of bone turnover, it cannot describe satisfactorily the complexity of the underlying biological crosstalk, highlighting the need of a more refined mechanobiological constitutive theory of bone turnover.

Keywords
Bone turnover, porosity, mineralization, generalized continuum mechanics, continuum thermodynamics

1. Introduction

Bone is a living material that can adapt to bear the superimposed mechanical forces and to respond to the chemical demands of the organism through a lifelong process known as bone remodeling. Bone remodeling can be investigated at different scales. At the macroscopic scale, bone remodeling emerges as an evolution of material properties, for instance via the increase/decrease of bone mass, reorientation (i.e., rotation) of material axes, and mineralization. At the microstructural scale, bone remodeling results from the action of several bone cells that work in concert to renew bone mass. Among others, osteoclasts (OC) remove bone matrix and osteoblasts (OB) lay down new, unmineralized bone matrix (commonly named osteoid) that further undergoes mineralization and transforms in mature, mineralized bone. The action of OC and OB is known to be coordinated by osteocytes (OT) [1]. Cell activity is regulated by complex autocrine and paracrine signaling related to the local biochemical and mechanical environment. In physiological conditions, the activity of OC and OB is balanced and there is no net change of bone mass. Several pathologies, e.g. osteoporosis, are related to unbalanced OC and OB activity. Understanding the mechanisms regulating bone remodeling and the crosstalk between cell populations is therefore of main importance to support clinical research and predict the mechanical properties of bone tissue.

Bone tissue is a composite organic material composed of collagen fibers, non-collagenous organic matter, inorganic salts, water, and mineral [2, 3]. While bone is built and resorbed by cells, the bone matrix itself contributes to the cellular metabolism, acting, for instance, as a reservoir of mineral that can be released into the fluid space [2,46]. There are two main types of bone tissue: cortical and trabecular tissue. Cortical bone is a dense and stiff structure that forms the outer layer of bones and is critical for the load-bearing function of the skeleton. Conversely, trabecular bone is a porous structure constituted by a network of rod-like and plate-like trabeculae.

Since the early observations in [7–10] in the second half of the 19th century, the link between mechanical loading and bone microstructure became apparent. In trabecular bone, this emerges as specific patterns of trabecular density (higher in highly stressed regions) and orientation (roughly aligned with the principal stress directions). The so-called Wolff's law, stating that the mechanical function of bone drives the evolution of its architecture, motivated a wealth of research work trying to explain the evolution of bone material in terms of different mechanical stimuli such as stress, strain, or strain energy density. Two major contributions in this domain are due to Cowin and Frost in the second half of the 20th century. In the 1970s and later decades, Cowin proposed several original models of bone remodeling linking the evolution of bone porosity and microarchitecture with mechanical principles [11, 12]. Shortly after, in the 1980s, Frost introduced the so-called "mechanostat theory" [13, 14] to describe the connection between bone remodeling and mechanics. This concept is still the keystone of several models of bone remodeling. Cowin and Frost's respective works paved the way to several biomechanical models investigating bone remodeling at the tissue level. Some of these works rely on optimization theories [15–18] or on *ad hoc* expressions of the evolution laws of the elastic moduli [19–22].

Several works investigated the evolution of living tissue drawing on the theory of continuum thermodynamics. Some models have been established in the framework of continuum damage mechanics [23–26]. A different approach has been proposed by Ganghoffer and coworkers in the framework of the thermodynamics of irreversible processes to describe bone internal and external remodeling [27]. Yet another approach has been proposed by DiCarlo in the early the 2000s encompassing both growth [28, 29] and remodeling [30]. This approach is set up in the framework of generalized continuum mechanics. Following [31], the kinematic description of a material point is enriched with additional parameters (sometimes referred to as *order parameters* [32]) related to its microstructure. A suitable statement of the virtual power principle is enforced to obtain the balance laws of the continuum which include both standard and generalized forces. Eventually, the evolution laws are obtained by introducing a suitable, thermodynamically consistent constitutive theory. This approach has already been applied to study the passive rotary remodeling of bone, i.e., the stress-driven rotation of the bone material

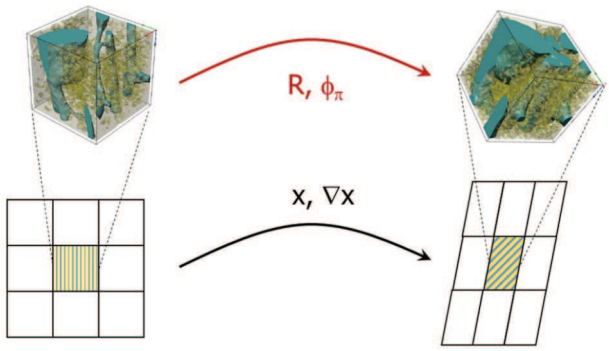

Figure 1. Continuum model of bone material undergoing deformation and remodeling. The cartoon on the bottom depicts the continuum description of bone orthotropic microstructure: at the continuum scale, details of the bone microstructure (insets on the top of the figure) are smeared out. The reference and deformed shapes are shown on the bottom-left and bottom-right, respectively. Top-left and top-right insets are enlarged views of the bone microstructure before and after remodeling. Gross deformation is described by the current placement and its gradient ($\mathbf{x}$, $\nabla\mathbf{x}$) of the material elements. Remodeling is described by the rotation of the material axes or microrotation (R) and change in material composition (ϕ_π, phase $\pi \in \{\mathrm{Por}, \mathrm{U}, \mathrm{M}\}$). See the text for details.

axes [33, 34]. In this paper, we extend this model to account also for *bone turnover*, i.e., the dynamic process of bone resorption (due to OC), formation of new, unmineralized bone (due to OB), and mineralization.

The main goal of this paper is thus to describe the general theory of a new bone remodeling model where two independent remodeling mechanisms are considered: the rotation of the material axes and the turnover of bone material. This is done in the first part of next section. After a description of the general ideas underlying our model, we set up the generalized kinematic description and balance laws. Then, the main ingredients of our constitutive theory (free energy and dissipation) are introduced to obtain the general form of the remodeling laws of the bone material. The second part of next section is focused on a toy model of bone turnover. Following a phenomenological approach, some simplifying constitutive assumptions are made in order to obtain simple mathematical laws of bone turnover. In doing so, we only aim at capturing the main features of bone turnover and do not pretend to be able to reproduce a realistic scenario. The descriptive capabilities of the turnover model are discussed in view of some numerical simulations focusing on either one or several turnover mechanisms. Based on a critical analysis of these results, we draw some conclusions and perspectives paving the way to set up a mechanobiological constitutive theory.

2. Continuum model of bone and bone turnover

We outline in this section the general ideas of our modeling approach to describe the remodeling process of cortical bone. Our model is framed in the theory of generalized continuum mechanics [31] and steps from the ideas set forth in [28] and further developed in [30, 33, 34]. In those works, the focus was set only on the stress-driven rotation of the material axes of bone material, the so-called rotary remodeling, whereas material composition was supposed not to change in time. Here, we extend this model to include the main features of bone turnover, i.e., the time evolution of bone composition.

2.1. General concept

Cortical bone is modeled at the tissue scale as an heterogeneous, porous material. Bone remodeling is encoded in the evolution of microstructural features such as composition (i.e., relative amount of constituent phases) and orientation of microstructure (to be called micro-orientation for short), see Figure 1.

Our modeling approach is set up in the framework of generalized continuum mechanics. Thus, microstructural features of bone material are smeared out at the continuum scale and described through suitable macroscopic kinematic variables. A three-phase continuum description is adopted here. Macroscopic pores (Haversian and Volkmann's canals, phase Por) are embedded in the bone matrix. The bone matrix is assumed to be constituted of an unmineralized (U) and a mineralized (M) phase. Moreover, phases are meant to be spatially organized so as to give bone an orthotropic material symmetry at the continuum scale. The material orthotropy directions are referred to as material axes throughout this paper.

Although our formalism includes both rotary remodeling and bone turnover, in this paper the focus is set on the latter. *Bone turnover* is basically related to two mechanisms: bone renewing (i.e., replacing old bone with new, unmineralized bone) and mineralization.

Bone renewing is mainly related to the action of osteoclasts (OC), cells responsible for bone resorption, and osteoblasts (OB), cells that lay down new bone. The action of OC and OB is orchestrated by the osteocytes (OT) and depends on complex biochemical interactions between those cell populations [35]. When the action of OC and OB is balanced, the total amount of porosity (phase Por) is stationary. However, if either the action of OC or OB prevails, an increase or decrease of porosity is observed, respectively.

The new bone laid down by the OB, usually named osteoid, is basically a collagen-rich gel. Osteoid (phase U) undergoes a progressive mineralization that may last several months and eventually lead to a fully mineralized matrix (phase M). *Mineralization* is a biochemical process (hereinafter referred to as χ) during which hydroxyapatite crystals nucleate between the collagen fibrils and develop replacing part of the water present in the osteoid [36]. For the sake of simplicity, the progressive mineralization of osteoid is not accounted for in our model and mineralization results in increasing the relative amount of phase M at the expense of phase U. (Vice versa, demineralization would result in increasing the relative amount of phase U at the expense of phase M.)

Here we aim at developing a continuum model of bone turnover. The heterogeneity emerging at the scale of bone microstructure is smeared out at the continuum scale where only the relative amounts of individual phases (Por, U, and M) matter in determining the mechanical properties of bone tissue. Nevertheless, it is useful to distinguish the contribution of each individual mechanism (OC, OB, and χ) taking place in bone turnover.

2.2. Kinematics and velocity

Working in the framework of generalized continuum mechanics, a material element of bone is described by its position in space enriched by additional parameters describing the current state of its microstructure.

Bone is represented by a continuous body $\mathfrak{B}$ occupying, at any time t, a regular region of the 3D Euclidean space $\mathcal{E}$. We identify the body $\mathfrak{B}$ with its reference shape Ω_0, i.e., the region that $\mathfrak{B}$ occupies at a reference time t_0, and a material element $\mathfrak{b} \in \mathfrak{B}$ with its reference position $\mathbf{X} \in \Omega_0$. As time goes by, the body deforms and its microstructure changes in terms of both micro-orientation and composition. (Hereinafter, a superposed dot will denote differentiation with respect to time.)

Visible deformation. The visible (or gross) deformation of a body element $\mathfrak{b}$ is described by its current position in space $\mathbf{x} \in \mathcal{E}$ or, equivalently, by its displacement $\mathbf{u} = \mathbf{x} - \mathbf{X} \in \mathsf{Vect}$, Vect being the tangent space of $\mathcal{E}$. The rate of change of $\mathbf{u}$ is the gross velocity $\mathbf{v} = \dot{\mathbf{u}} \in \mathsf{Vect}$.

Micro-orientation. Bone micro-orientation is encoded at the continuum scale in the orientation of the bone material axes. Thus, although micro-orientation and orientation of material axes refer to different scales, the two terms will be used synonymously hereinafter for the sake of concision. In line with [30], the micro-orientation is described by a second-order rotation tensor $\mathrm{R} \in \mathsf{Orth}^+$ (Orth^+ being the space of the second-order rotation tensors). The rate of change of the micro-orientation is measured by the skew-symmetric, second-order tensor $\mathrm{V} = \dot{\mathrm{R}}\mathrm{R}^{\mathrm{T}} \in \mathsf{Skw}$ representing the rotary remodeling velocity (Skw being the space of the second-order, skew-symmetric tensors and superscript $^{\mathrm{T}}$ denoting transposition).

Composition. The composition of a bone volume element is measured by the volume fractions ϕ_{Por}, ϕ_{U}, and ϕ_{M} of porosity (phase Por), unmineralized (U) and mineralized (M) bone matrix, respectively. The volume fraction of phase $\pi \in \{\mathsf{Por}, \mathsf{U}, \mathsf{M}\}$ is defined as the ratio between the volume of the phase π and the total volume: $\phi_\pi \overset{\text{def}}{=} Vol_\pi / Vol_{tot} \in [0, 1]$. The actual values of the volume fractions result from the history of the three turnover mechanisms described before (OB, OC, and χ). For instance, the actual value of porosity results from the total volume of bone resorbed and laid down over time by the OC and OB, respectively. It is not meaningful to follow these total volumes over time. However, it is important to describe the rate of change of the volume fractions in terms of the relevant turnover mechanisms. At any time, the sum of the volume fractions must be equal to one:

$$\phi_{\mathsf{Por}} + \phi_{\mathsf{U}} + \phi_{\mathsf{M}} = 1. \tag{1}$$

Therefore, in the following, only ϕ_{U} and ϕ_{M} will be considered as independent variables whereas the value of ϕ_{Por} will be deduced as $\phi_{\mathsf{Por}} = 1 - \phi_{\mathsf{U}} - \phi_{\mathsf{M}}$. Looking at Figure 2, it is apparent that the volume

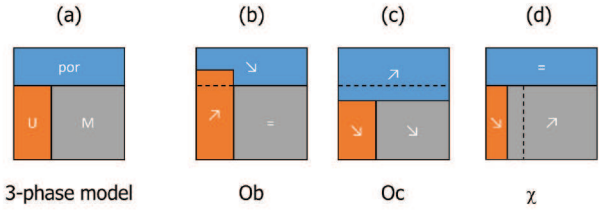

Figure 2. (a) Three-phase model of bone material: U: unmineralized bone, M: mineralized bone, and Por: porosity; Remodeling mechanisms: (b) Osteoblasts (OB) lay down new, unmineralized bone; (c) Osteoclasts (OC) remove bone; and (d) Mineralization (χ) transforms unmineralized bone in mineralized bone.

of unmineralized bone (U-bone) can change owing to three mechanisms (OB, OC, and χ) whereas the volume of mineralized bone (M-bone) can change owing to two mechanisms (OC and χ), reading

$$\dot{\phi}_{\mathsf{U}} = \dot{\phi}_{\mathsf{U}}^{\mathsf{OB}} + \dot{\phi}_{\mathsf{U}}^{\mathsf{OC}} + \dot{\phi}_{\mathsf{U}}^{\chi}, \tag{2}$$

$$\dot{\phi}_{\mathsf{M}} = \dot{\phi}_{\mathsf{M}}^{\mathsf{OC}} + \dot{\phi}_{\mathsf{M}}^{\chi}, \tag{3}$$

where $\dot{\phi}_{\pi}^{\varpi}$ expresses the rate of change of the volume fraction of phase π owing to the mechanism ϖ. Then, the complete turnover velocity is expressed by the set of individual velocities $\left(\dot{\phi}_{\mathsf{U}}^{\mathsf{OB}}, \dot{\phi}_{\mathsf{U}}^{\mathsf{OC}}, \dot{\phi}_{\mathsf{U}}^{\chi}, \dot{\phi}_{\mathsf{M}}^{\mathsf{OC}}, \dot{\phi}_{\mathsf{M}}^{\chi}\right) \in \mathbb{R}^5$. Note that OB and OC are expected to contribute positively and negatively, respectively, to the rates of volume fractions: $\dot{\phi}_{\mathsf{U}}^{\mathsf{OB}} > 0$ and $\dot{\phi}_{\mathsf{U}}^{\mathsf{OC}}, \dot{\phi}_{\mathsf{M}}^{\mathsf{OC}} < 0$. Moreover, mineralization is expected to contribute evenly but with opposite sign to the rates of mineralized and unmineralized bone volume fractions: $\dot{\phi}_{\mathsf{M}}^{\chi} = -\dot{\phi}_{\mathsf{U}}^{\chi} > 0$. (Demineralization can be also described by changing the sign of this inequality.)

In the end, the instantaneous evolution of $\mathfrak{b}$ is expressed by the *complete velocity*: $\mathcal{V} = \left(\mathbf{v}, \mathrm{V}, v_{\mathsf{U}}^{\mathsf{OB}}, v_{\mathsf{U}}^{\mathsf{OC}}, v_{\mathsf{U}}^{\chi}, v_{\mathsf{M}}^{\mathsf{OC}}, v_{\mathsf{M}}^{\chi}\right)$, where we noted $v_{\pi}^{\varpi} = \dot{\phi}_{\pi}^{\varpi}$.

2.3. Balance and forces

The generalized balance equations ruling the evolution of the body $\mathfrak{B}$ are obtained by a suitable statement of the principle of virtual power. According to the above expression of the complete velocity, we postulate the following expressions for the inner and outer power expended on a body part $\Pi_0 \subseteq \Omega_0$:

$$\overset{\mathrm{i}}{\mathcal{P}}(\mathcal{V}) = \int_{\Pi_0} -\mathrm{S}\cdot\nabla\mathbf{v} + \overset{\mathrm{i}}{\mathrm{T}}\cdot\mathrm{V} + \overset{\mathrm{i}}{\lambda}_{\mathsf{U}}^{\mathsf{OB}} v_{\mathsf{U}}^{\mathsf{OB}} + \overset{\mathrm{i}}{\lambda}_{\mathsf{U}}^{\mathsf{OC}} v_{\mathsf{U}}^{\mathsf{OC}} + \overset{\mathrm{i}}{\lambda}_{\mathsf{U}}^{\chi} v_{\mathsf{U}}^{\chi} + \overset{\mathrm{i}}{\lambda}_{\mathsf{M}}^{\mathsf{OC}} v_{\mathsf{M}}^{\mathsf{OC}} + \overset{\mathrm{i}}{\lambda}_{\mathsf{M}}^{\chi} v_{\mathsf{M}}^{\chi}, \tag{4}$$

$$\overset{\mathrm{o}}{\mathcal{P}}(\mathcal{V}) = \int_{\Pi_0} -\mathbf{b}\cdot\mathbf{v} + \overset{\mathrm{o}}{\mathrm{T}}\cdot\mathrm{V} + \overset{\mathrm{o}}{\lambda}_{\mathsf{U}}^{\mathsf{OB}} v_{\mathsf{U}}^{\mathsf{OB}} + \overset{\mathrm{o}}{\lambda}_{\mathsf{U}}^{\mathsf{OC}} v_{\mathsf{U}}^{\mathsf{OC}} + \overset{\mathrm{o}}{\lambda}_{\mathsf{U}}^{\chi} v_{\mathsf{U}}^{\chi} + \overset{\mathrm{o}}{\lambda}_{\mathsf{M}}^{\mathsf{OC}} v_{\mathsf{M}}^{\mathsf{OC}} + \overset{\mathrm{o}}{\lambda}_{\mathsf{M}}^{\chi} v_{\mathsf{M}}^{\chi} + \int_{\partial\Pi_0} \mathbf{f}\cdot\mathbf{v}, \tag{5}$$

where $\partial\Pi_0$ is the boundary of Π_0, ∇ is the gradient operator and a centered dot denotes the inner product in the appropriate space. The inner and outer powers represent the power expended by the generalized inner and outer forces, respectively, for the velocity $\mathcal{V}$. In the expression of the inner power $\overset{\mathrm{i}}{\mathcal{P}}$ there appear the stress tensor $\mathrm{S} \in$ Sym (Sym being the space of second-order, symmetric tensors) and the generalized inner forces related to remodeling. In the expression of the outer power $\overset{\mathrm{o}}{\mathcal{P}}$ there appear the gross body and boundary forces ($\mathbf{b}$ and $\mathbf{f}$, respectively) and the generalized outer forces related to remodeling. The rotary remodeling inner and outer couples $\overset{\mathrm{i}}{\mathrm{T}}, \overset{\mathrm{o}}{\mathrm{T}} \in$ Skw are associated with the evolution of the micro-orientation. The inner and outer turnover forces $\overset{\mathrm{i}}{\lambda}_{\pi}^{\varpi}, \overset{\mathrm{o}}{\lambda}_{\pi}^{\varpi} \in \mathbb{R}$ (with $\pi \in \{\mathsf{U}, \mathsf{M}\}$ and $\varpi \in \{\mathsf{OB}, \mathsf{OC}, \chi\}$) are associated with the evolution of the volume fractions of phase π owing to the turnover mechanism ϖ.

Let $\tilde{\mathcal{V}} = \left(\tilde{\mathbf{v}}, \tilde{\mathrm{V}}, \tilde{v}_{\mathsf{U}}^{\mathsf{OB}}, \tilde{v}_{\mathsf{U}}^{\mathsf{OC}}, \tilde{v}_{\mathsf{U}}^{\chi}, \tilde{v}_{\mathsf{M}}^{\mathsf{OC}}, \tilde{v}_{\mathsf{M}}^{\chi}\right)$ be the *complete test velocity* associated with $\mathcal{V}$. Following [30], we require the total power to be null for any complete test velocity $\tilde{\mathcal{V}}$ and any body part Π_0:

$$\mathcal{P}(\tilde{\mathcal{V}}) = \overset{\mathrm{i}}{\mathcal{P}}(\tilde{\mathcal{V}}) + \overset{\mathrm{o}}{\mathcal{P}}(\tilde{\mathcal{V}}) = 0 \quad \forall\tilde{\mathcal{V}}\,\&\,\forall\Pi_0. \tag{6}$$

Thus, standard localization arguments allow one to obtain the local statements of the generalized balance equations (i.e., related to the gross deformation of the body and to the different mechanisms considered in our kinematic description of bone remodeling) that must hold at any body point and any time. On the one hand, the gross bulk and boundary balance equations read

$$\mathrm{Div}\mathrm{S} + \mathbf{b} = 0 \quad \text{in}\,\Omega_0, \qquad \mathrm{S}\cdot\mathbf{n} = \mathbf{f} \quad \text{on}\,\partial\Omega_0. \tag{7}$$

On the other hand, the balance equations related to remodeling read:

$$\overset{\mathrm{i}}{\mathrm{T}} + \overset{\mathrm{o}}{\mathrm{T}} = 0, \tag{8}$$

$$\overset{\mathrm{i}}{\lambda}{}^{\mathsf{OB}}_{\mathsf{U}} + \overset{\mathrm{o}}{\lambda}{}^{\mathsf{OB}}_{\mathsf{U}} = 0, \tag{9}$$

$$\overset{\mathrm{i}}{\lambda}{}^{\mathsf{OC}}_{\mathsf{U}} + \overset{\mathrm{o}}{\lambda}{}^{\mathsf{OC}}_{\mathsf{U}} = 0, \tag{10}$$

$$\overset{\mathrm{i}}{\lambda}{}^{\mathsf{OC}}_{\mathsf{M}} + \overset{\mathrm{o}}{\lambda}{}^{\mathsf{OC}}_{\mathsf{M}} = 0, \tag{11}$$

$$\Delta\overset{\mathrm{i}}{\lambda}{}^{\chi} + \Delta\overset{\mathrm{o}}{\lambda}{}^{\chi} = 0, \tag{12}$$

with $\Delta\overset{\mathrm{i}}{\lambda}{}^{\chi} \overset{\text{def}}{=} \overset{\mathrm{i}}{\lambda}{}^{\chi}_{\mathsf{M}} - \overset{\mathrm{i}}{\lambda}{}^{\chi}_{\mathsf{U}}$ and $\Delta\overset{\mathrm{o}}{\lambda}{}^{\chi} \overset{\text{def}}{=} \overset{\mathrm{o}}{\lambda}{}^{\chi}_{\mathsf{M}} - \overset{\mathrm{o}}{\lambda}{}^{\chi}_{\mathsf{U}}$. Equations (8-12) hold in Ω_0. There are no boundary balance equations related to remodeling since only the remodeling velocities (and not their gradients) enter the expressions of the powers in Equations (4-5). Moreover, Equation (12) has been obtained by taking into account the kinematic constraint $\tilde{v}^{\chi}_{\mathsf{U}} + \tilde{v}^{\chi}_{\mathsf{M}} = 0$.

The remodeling stimuli exerted by the biochemical environment emerge in this model through the generalized outer forces (having the physical dimensions of energy per unit volume). Each remodeling stimulus represents the energy supply made available to bone that is directly targeted to a specific remodeling pathway. No thermodynamic restrictions hold on the expressions of these stimuli. By contrast, inner forces shall be constitutively related to the kinematic descriptors of bone in a thermodynamically consistent way.

Equations (8-12), supplemented with suitable constitutive assumptions for the inner forces, encode the remodeling laws of the system. Inner forces can have both reversible (energetic) and irreversible (dissipative) components. These features are addressed in the following section.

2.4. Constitutive theory

We develop our constitutive theory so as to ensure the thermodynamic compatibility of our model. First, we postulate an expression for the free energy of the system. Then, a suitable statement of the dissipation principle is used to retrieve the remodeling laws of the system.

Free energy. We assume the existence of a free energy density function ψ being the sum of a mechanical and a biochemical contribution:

$$\psi = \psi_{\mathsf{mech}} + \psi_{\mathsf{chem}}. \tag{13}$$

We postulate the mechanical contribution ψ_{mech} to be a quadratic function of the small strain tensor:

$$\psi_{\mathsf{mech}} = \widehat{\psi}_{\mathsf{mech}}\,(\mathrm{E}, \mathrm{R}, \phi_{\mathsf{U}}, \phi_{\mathsf{M}}) = \frac{1}{2}\,\mathbb{C}\mathrm{E}\cdot\mathrm{E}, \tag{14}$$

where $\mathrm{E} = \mathsf{sym}\nabla\mathbf{u}$ is the gross (small) strain tensor and $\mathbb{C} = \widehat{\mathbb{C}}\,(\mathrm{R}, \phi_{\mathsf{U}}, \phi_{\mathsf{M}})$ the fourth-order elasticity tensor. The latter depends on the orientation (R) and composition (ϕ_{U}, ϕ_{M}) of the microstructure. Assuming the material to be orthotropic, the elasticity tensor can be expressed as a prototype tensor $\mathbb{C}_0 = \widehat{\mathbb{C}}_0\,(\phi_{\mathsf{U}}, \phi_{\mathsf{M}})$ (whose orthotropy axes are aligned with a fixed frame) rotated by R to account for the actual micro-orientation:

$$\mathbb{C} = \mathbb{R}\mathbb{C}_0\mathbb{R}^{\mathrm{T}}, \tag{15}$$

where $\mathbb{R}$ is the fourth-order rotation tensor associated with R (see, e.g., [37]).

The biochemical energy density ψ_{chem} is assumed to be the sum of phase-specific contributions:

$$\psi_{\mathsf{chem}} = \widehat{\psi}_{\mathsf{chem}}\left(\phi_{\mathsf{U}}, \phi_{\mathsf{M}}\right) = \sum_{\pi \in \{\mathsf{Por},\mathsf{U},\mathsf{M}\}} \phi_\pi \, \mu_\pi, \tag{16}$$

where μ_π is the chemical potential of phase π. Recalling that the volume fractions must sum to one, ψ_{chem} can read

$$\psi_{\mathsf{chem}} = \mu_{\mathsf{Por}} + \left(\mu_{\mathsf{U}} - \mu_{\mathsf{Por}}\right) \phi_{\mathsf{U}} + \left(\mu_{\mathsf{M}} - \mu_{\mathsf{Por}}\right) \phi_{\mathsf{M}}. \tag{17}$$

We make the standard assumption that the chemical potential of the solid phases is constant. The chemical potential of the Por phase can change according to the ionic force of the interstitial fluid. However, this physical dependency does not appear directly in our model. In particular, μ_{Por} is assumed not to depend on the volume fractions ϕ_{U} and ϕ_{M}. Therefore, the energy ψ_{chem} turns out to be a linear function of the volume fractions.

Dissipation principle. A suitable statement of the dissipation principle is enforced to select the thermodynamic compatible evolutions of our model. The dissipation principle states that, along any actual deformation of the system, the outer power shall exceed the rate of change of the free energy:

$$\overset{+}{\mathcal{P}} \overset{\text{def}}{=} \overset{\circ}{\mathcal{P}} - \dot{\psi} = -\overset{\imath}{\mathcal{P}} - \dot{\psi} \geq 0, \tag{18}$$

where $\overset{+}{\mathcal{P}}$ represents the power dissipated during the evolution of the system and the second equality results from the balance of inner and outer powers. In view of Equation (4) and Equation (13), the generalized dissipation principle reads

$$\overset{+}{\mathcal{P}} = \mathrm{S} \cdot \nabla \mathbf{v} - \overset{\imath}{\mathrm{T}} \cdot \mathrm{V} - \overset{\imath}{\lambda}{}_{\mathsf{U}}^{\mathsf{OB}} \, \nu_{\mathsf{U}}^{\mathsf{OB}} - \overset{\imath}{\lambda}{}_{\mathsf{U}}^{\mathsf{OC}} \, \nu_{\mathsf{U}}^{\mathsf{OC}} - \overset{\imath}{\lambda}{}_{\mathsf{M}}^{\mathsf{OC}} \, \nu_{\mathsf{M}}^{\mathsf{OC}} - \Delta\overset{\imath}{\lambda}{}^{\chi} \, \nu_{\mathsf{M}}^{\chi} - \dot{\psi}_{\mathsf{mech}} - \dot{\psi}_{\mathsf{chem}} \geq 0. \tag{19}$$

In view of Equation (14), the rate of ψ_{mech} reads

$$\dot{\psi}_{\mathsf{mech}} = \mathbb{C}\mathrm{E} \cdot \dot{\mathrm{E}} - [\mathbb{C}\mathrm{E}, \mathrm{E}] \cdot \dot{\mathrm{R}}\mathrm{R}^{\mathrm{T}} + \frac{1}{2}\left(\frac{\partial \mathbb{C}}{\partial \phi_{\mathsf{U}}}\mathrm{E} \cdot \mathrm{E}\right) \dot{\phi}_{\mathsf{U}} + \frac{1}{2}\left(\frac{\partial \mathbb{C}}{\partial \phi_{\mathsf{M}}}\mathrm{E} \cdot \mathrm{E}\right) \dot{\phi}_{\mathsf{M}}, \tag{20}$$

where the brackets denote the commutation operator between second-order tensors: $[\mathrm{A}, \mathrm{B}] = \mathrm{AB} - \mathrm{BA}$. The expressions of the first and second terms in the above expression have been obtained in [30] and do not change in our context when introducing the volume fractions in the list of arguments of ψ_{mech} (Equation (14)). It is worth noting that, if the gross strain is null $\mathrm{E} = 0$, $\dot{\psi}_{\mathsf{mech}}$ is null as well.

In view of Equation (17), the rate of ψ_{chem} reads

$$\dot{\psi}_{\mathsf{chem}} = \frac{\partial \psi_{\mathsf{chem}}}{\partial \phi_{\mathsf{U}}} \dot{\phi}_{\mathsf{U}} + \frac{\partial \psi_{\mathsf{chem}}}{\partial \phi_{\mathsf{M}}} \dot{\phi}_{\mathsf{M}} = \left(\mu_{\mathsf{U}} - \mu_{\mathsf{Por}}\right) \dot{\phi}_{\mathsf{U}} + \left(\mu_{\mathsf{M}} - \mu_{\mathsf{Por}}\right) \dot{\phi}_{\mathsf{M}}. \tag{21}$$

Introducing Equations (20-21) and Equations (2-3) in Equation (19), the dissipation inequality can be rewritten as

$$\overset{+}{\mathcal{P}} = \overset{+}{\mathrm{S}} \cdot \dot{\mathrm{E}} + \overset{+}{\mathrm{T}} \cdot \dot{\mathrm{R}}\mathrm{R}^{\mathrm{T}} + \overset{+}{\lambda}{}_{\mathsf{U}}^{\mathsf{OB}} \, \dot{\phi}_{\mathsf{U}}^{\mathsf{OB}} + \overset{+}{\lambda}{}_{\mathsf{U}}^{\mathsf{OC}} \, \dot{\phi}_{\mathsf{U}}^{\mathsf{OC}} + \overset{+}{\lambda}{}_{\mathsf{U}}^{\chi} \, \dot{\phi}_{\mathsf{U}}^{\chi} + \overset{+}{\lambda}{}_{\mathsf{M}}^{\mathsf{OC}} \, \dot{\phi}_{\mathsf{M}}^{\mathsf{OC}} + \overset{+}{\lambda}{}_{\mathsf{M}}^{\chi} \, \dot{\phi}_{\mathsf{M}}^{\chi} \geq 0, \tag{22}$$

where we introduced the generalized *dissipative forces*:

$$\overset{+}{\mathrm{S}} \overset{\text{def}}{=} \mathrm{S} - \mathbb{C}\mathrm{E}, \tag{23}$$

$$\overset{+}{\mathrm{T}} \overset{\text{def}}{=} -\overset{\imath}{\mathrm{T}} + [\mathbb{C}\mathrm{E}, \mathrm{E}] = \overset{\circ}{\mathrm{T}} + [\mathbb{C}\mathrm{E}, \mathrm{E}], \tag{24}$$

$$\overset{+}{\lambda}{}_{\mathsf{U}}^{\mathsf{OB}} \overset{\text{def}}{=} -\overset{\imath}{\lambda}{}_{\mathsf{U}}^{\mathsf{OB}} - \overset{\psi}{\lambda}_{\mathsf{U}} = \overset{\circ}{\lambda}{}_{\mathsf{U}}^{\mathsf{OB}} - \overset{\psi}{\lambda}_{\mathsf{U}}, \tag{25}$$

$$\overset{+}{\lambda}{}^{\mathsf{OC}}_{\mathsf{U}} \overset{\text{def}}{=} -\overset{i}{\lambda}{}^{\mathsf{OC}}_{\mathsf{U}} - \overset{\Psi}{\lambda}_{\mathsf{U}} = \overset{\circ}{\lambda}{}^{\mathsf{OC}}_{\mathsf{U}} - \overset{\Psi}{\lambda}_{\mathsf{U}}, \tag{26}$$

$$\overset{+}{\lambda}{}^{\chi}_{\mathsf{U}} \overset{\text{def}}{=} -\overset{i}{\lambda}{}^{\chi}_{\mathsf{U}} - \overset{\Psi}{\lambda}_{\mathsf{U}} = \overset{\circ}{\lambda}{}^{\chi}_{\mathsf{U}} - \overset{\Psi}{\lambda}_{\mathsf{U}}, \tag{27}$$

$$\overset{+}{\lambda}{}^{\mathsf{OC}}_{\mathsf{M}} \overset{\text{def}}{=} -\overset{i}{\lambda}{}^{\mathsf{OC}}_{\mathsf{M}} - \overset{\Psi}{\lambda}_{\mathsf{M}} = \overset{\circ}{\lambda}{}^{\mathsf{OC}}_{\mathsf{M}} - \overset{\Psi}{\lambda}_{\mathsf{M}}, \tag{28}$$

$$\overset{+}{\lambda}{}^{\chi}_{\mathsf{M}} \overset{\text{def}}{=} -\overset{i}{\lambda}{}^{\chi}_{\mathsf{M}} - \overset{\Psi}{\lambda}_{\mathsf{M}} = \overset{\circ}{\lambda}{}^{\chi}_{\mathsf{M}} - \overset{\Psi}{\lambda}_{\mathsf{M}}, \tag{29}$$

where we set

$$\overset{\Psi}{\lambda}_{\mathsf{U}} \overset{\text{def}}{=} \overset{\Psi}{\lambda}{}^{\mathsf{mech}}_{\mathsf{U}} + \overset{\Psi}{\lambda}{}^{\mathsf{chem}}_{\mathsf{U}}, \qquad \overset{\Psi}{\lambda}{}^{\mathsf{mech}}_{\mathsf{U}} \overset{\text{def}}{=} \frac{1}{2}\frac{\partial \mathbb{C}}{\partial \phi_{\mathsf{U}}}\mathrm{E}\cdot\mathrm{E}, \qquad \overset{\Psi}{\lambda}{}^{\mathsf{chem}}_{\mathsf{U}} \overset{\text{def}}{=} \mu_{\mathsf{U}} - \mu_{\mathsf{Por}}, \tag{30}$$

$$\overset{\Psi}{\lambda}_{\mathsf{M}} \overset{\text{def}}{=} \overset{\Psi}{\lambda}{}^{\mathsf{mech}}_{\mathsf{M}} + \overset{\Psi}{\lambda}{}^{\mathsf{chem}}_{\mathsf{M}}, \qquad \overset{\Psi}{\lambda}{}^{\mathsf{mech}}_{\mathsf{M}} \overset{\text{def}}{=} \frac{1}{2}\frac{\partial \mathbb{C}}{\partial \phi_{\mathsf{M}}}\mathrm{E}\cdot\mathrm{E}, \qquad \overset{\Psi}{\lambda}{}^{\mathsf{chem}}_{\mathsf{M}} \overset{\text{def}}{=} \mu_{\mathsf{M}} - \mu_{\mathsf{Por}}. \tag{31}$$

Recalling the kinematic constraint $\dot{\phi}^{\chi}_{\mathsf{U}} + \dot{\phi}^{\chi}_{\mathsf{M}} = 0$, the two terms related to the mineralization in Equation (22) can be collapsed as

$$\overset{+}{\lambda}{}^{\chi}_{\mathsf{U}}\,\dot{\phi}^{\chi}_{\mathsf{U}} + \overset{+}{\lambda}{}^{\chi}_{\mathsf{M}}\,\dot{\phi}^{\chi}_{\mathsf{M}} = \Delta\overset{+}{\lambda}{}^{\chi}\,\dot{\phi}^{\chi}_{\mathsf{M}}, \tag{32}$$

where the effective dissipative force related to mineralization has been introduced:

$$\Delta\overset{+}{\lambda}{}^{\chi} \overset{\text{def}}{=} \overset{+}{\lambda}{}^{\chi}_{\mathsf{M}} - \overset{+}{\lambda}{}^{\chi}_{\mathsf{U}} = \left(\overset{\circ}{\lambda}{}^{\chi}_{\mathsf{M}} - \overset{\circ}{\lambda}{}^{\chi}_{\mathsf{U}}\right) - \left(\overset{\Psi}{\lambda}_{\mathsf{M}} - \overset{\Psi}{\lambda}_{\mathsf{U}}\right) = \left(\overset{\circ}{\lambda}{}^{\chi}_{\mathsf{M}} - \overset{\circ}{\lambda}{}^{\chi}_{\mathsf{U}}\right) - \left(\overset{\Psi}{\lambda}{}^{\mathsf{mech}}_{\mathsf{M}} - \overset{\Psi}{\lambda}{}^{\mathsf{mech}}_{\mathsf{U}}\right) - \left(\overset{\Psi}{\lambda}{}^{\mathsf{chem}}_{\mathsf{M}} - \overset{\Psi}{\lambda}{}^{\mathsf{chem}}_{\mathsf{U}}\right). \tag{33}$$

Setting

$$\Delta\overset{\circ}{\lambda}{}^{\chi} \overset{\text{def}}{=} \overset{\circ}{\lambda}{}^{\chi}_{\mathsf{M}} - \overset{\circ}{\lambda}{}^{\chi}_{\mathsf{U}}, \tag{34}$$

$$\Delta\overset{\Psi}{\lambda}{}^{\mathsf{mech}} \overset{\text{def}}{=} \overset{\Psi}{\lambda}{}^{\mathsf{mech}}_{\mathsf{M}} - \overset{\Psi}{\lambda}{}^{\mathsf{mech}}_{\mathsf{U}} = \frac{1}{2}\left(\frac{\partial \mathbb{C}}{\partial \phi_{\mathsf{M}}}\mathrm{E} - \frac{\partial \mathbb{C}}{\partial \phi_{\mathsf{U}}}\mathrm{E}\right)\cdot\mathrm{E}, \tag{35}$$

$$\Delta\overset{\Psi}{\lambda}{}^{\mathsf{chem}} \overset{\text{def}}{=} \overset{\Psi}{\lambda}{}^{\mathsf{chem}}_{\mathsf{M}} - \overset{\Psi}{\lambda}{}^{\mathsf{chem}}_{\mathsf{U}} = \mu_{\mathsf{M}} - \mu_{\mathsf{U}}, \tag{36}$$

the expression of $\Delta\overset{+}{\lambda}{}^{\chi}$ reads

$$\Delta\overset{+}{\lambda}{}^{\chi} = \Delta\overset{\circ}{\lambda}{}^{\chi} - \Delta\overset{\Psi}{\lambda}{}^{\mathsf{mech}} - \Delta\overset{\Psi}{\lambda}{}^{\mathsf{chem}}. \tag{37}$$

Equation (37) highlights that the dissipation related to mineralization comes from the difference between the effective external stimulus $\Delta\overset{\circ}{\lambda}{}^{\chi}$ triggering the $\mathsf{U} \to \mathsf{M}$ transition and the change of free energy of the system associated to this transition. More precisely, the terms $\Delta\overset{\Psi}{\lambda}{}^{\mathsf{mech}}$ and $\Delta\overset{\Psi}{\lambda}{}^{\mathsf{chem}}$ encode the change in strain and chemical energy, respectively, associated with the rate of transition of the solid matrix from an unmineralized to a mineralized state. As the phase M is stiffer than the phase U, the term $\Delta\overset{\Psi}{\lambda}{}^{\mathsf{mech}}$ is expected to be positive. Moreover, As the phase M is more stable than the phase U in regular conditions, the chemical potential of the former is expected to be lower than that of the latter and the term $\Delta\overset{\Psi}{\lambda}{}^{\mathsf{chem}}$ is expected to be negative.

As, in addition to remodeling, the material is assumed to behave as a linearly elastic medium, no dissipation is associated to the macroscopic stress and strain ($\overset{+}{\mathrm{S}} = 0$) and Equation (23) leads to the classical elasticity law $\mathrm{S} = \mathbb{C}\mathrm{E}$. The reduced dissipation inequality eventually reads

$$\overset{+}{\mathcal{P}} = \overset{+}{\mathrm{T}}\cdot\dot{\mathrm{R}}\mathrm{R}^{\mathrm{T}} + \overset{+}{\lambda}{}^{\mathsf{OB}}_{\mathsf{U}}\,\dot{\phi}^{\mathsf{OB}}_{\mathsf{U}} + \overset{+}{\lambda}{}^{\mathsf{OC}}_{\mathsf{U}}\,\dot{\phi}^{\mathsf{OC}}_{\mathsf{U}} + \overset{+}{\lambda}{}^{\mathsf{OC}}_{\mathsf{M}}\,\dot{\phi}^{\mathsf{OC}}_{\mathsf{M}} + \Delta\overset{+}{\lambda}{}^{\chi}\,\dot{\phi}^{\chi}_{\mathsf{M}} \geq 0, \tag{38}$$

where only the independent dissipation mechanisms related to bone remodeling appear.

Remodeling laws. The expression of the dissipative remodeling forces shall be specified in such a way to satisfy the reduced dissipation principle, Equation (38). For the sake of simplicity, we assume each dissipative force to be proportional to the corresponding remodeling velocity, reading

$$\overset{+}{\mathrm{T}} = \mathbb{D}(\dot{\mathrm{R}}\mathrm{R}^{\mathrm{T}}), \tag{39}$$

$$\overset{+}{\lambda}{}^{\mathsf{OB}}_{\mathsf{U}} = d^{\mathsf{OB}}_{\mathsf{U}}\,\dot{\phi}^{\mathsf{OB}}_{\mathsf{U}}, \tag{40}$$

$$\overset{+}{\lambda}{}^{\mathsf{OC}}_{\mathsf{U}} = d^{\mathsf{OC}}_{\mathsf{U}}\,\dot{\phi}^{\mathsf{OC}}_{\mathsf{U}}, \tag{41}$$

$$\overset{+}{\lambda}{}^{\mathsf{OC}}_{\mathsf{M}} = d^{\mathsf{OC}}_{\mathsf{M}}\,\dot{\phi}^{\mathsf{OC}}_{\mathsf{M}}, \tag{42}$$

$$\Delta\overset{+}{\lambda}{}^{\chi} = d^{\chi}\,\dot{\phi}^{\chi}_{\mathsf{M}}, \tag{43}$$

where $\mathbb{D}$ is a fourth-order dissipation tensor such as $\mathbb{D}\mathrm{W}\cdot\mathrm{W} \geq 0\,\forall \mathrm{W} \in \mathsf{Skw}$, to be called rotary remodeling resistance, and $d^{\varpi}_{\pi} \in \mathbb{R}^{+}$ are positive dissipation coefficients, in the following to be called *turnover resistances*. Introducing the above expressions of the dissipative forces in Equations (24), (25), (26), (28), and (37), the following remodeling laws are readily obtained:

$$\mathbb{D}(\dot{\mathrm{R}}\mathrm{R}^{\mathrm{T}}) = \overset{\circ}{\mathrm{T}} + [\mathbb{C}\mathrm{E}, \mathrm{E}]\,, \tag{44}$$

$$d^{\mathsf{OB}}_{\mathsf{U}}\,\dot{\phi}^{\mathsf{OB}}_{\mathsf{U}} = \overset{\circ}{\lambda}{}^{\mathsf{OB}}_{\mathsf{U}} - \overset{\psi}{\lambda}{}^{\mathsf{mech}}_{\mathsf{U}} - \overset{\psi}{\lambda}{}^{\mathsf{chem}}_{\mathsf{U}}, \tag{45}$$

$$d^{\mathsf{OC}}_{\mathsf{U}}\,\dot{\phi}^{\mathsf{OC}}_{\mathsf{U}} = \overset{\circ}{\lambda}{}^{\mathsf{OC}}_{\mathsf{U}} - \overset{\psi}{\lambda}{}^{\mathsf{mech}}_{\mathsf{U}} - \overset{\psi}{\lambda}{}^{\mathsf{chem}}_{\mathsf{U}}, \tag{46}$$

$$d^{\mathsf{OC}}_{\mathsf{M}}\,\dot{\phi}^{\mathsf{OC}}_{\mathsf{M}} = \overset{\circ}{\lambda}{}^{\mathsf{OC}}_{\mathsf{M}} - \overset{\psi}{\lambda}{}^{\mathsf{mech}}_{\mathsf{M}} - \overset{\psi}{\lambda}{}^{\mathsf{chem}}_{\mathsf{M}}, \tag{47}$$

$$d^{\chi}\,\dot{\phi}^{\chi}_{\mathsf{M}} = \Delta\overset{\circ}{\lambda}{}^{\chi} - \Delta\overset{\psi}{\lambda}{}^{\mathsf{mech}} - \Delta\overset{\psi}{\lambda}{}^{\mathsf{chem}}. \tag{48}$$

Equation (44) governs bone rotary remodeling and Equations (45-48) govern bone turnover. We emphasize that the quantities $\phi^{\varpi}_{\pi} = \int \dot{\phi}^{\varpi}_{\pi}\,dt$ are *not* volume fractions and have no interest *per se*. The relevant information comes from the sum of the individual turnover mechanisms, as per Equations (2-3), that compete with each other in determining the evolution of the volume fractions of porosity, unmineralized and mineralized matrix. However, if need be, we refer to these quantities as pseudo-volume fractions.

2.5. Bone turnover

In the following, we focus only on the equations and parameters related to bone turnover. Note that all the remodeling laws related to bone turnover, Equations (45-48), are scalar equations that admit the following representation:

$$\dot{\phi} = \frac{1}{d}\left(\overset{\circ}{\lambda} - \overset{\psi}{\lambda}\right), \tag{49}$$

where $\overset{\mathrm{n}}{\lambda} \overset{\mathrm{def}}{=} \overset{\circ}{\lambda} - \overset{\psi}{\lambda}$ represents the *net* turnover stimulus. The expressions of the inner actions $\overset{\psi}{\lambda}$ being provided by the derivatives of the free energy, suitable expressions for the turnover resistances d and outer stimuli $\overset{\circ}{\lambda}$ shall be provided in order to solve the above remodeling laws.

Turnover resistances. The turnover resistances $d^{\mathsf{OB}}_{\mathsf{U}}$, $d^{\mathsf{OC}}_{\mathsf{U}}$, $d^{\mathsf{OC}}_{\mathsf{M}}$, and d^{χ} are time-dependent, positive-valued coefficients modulating the effects of the associated net turnover stimuli: the higher the turnover resistance, the slower the associated turnover velocity (for a given net turnover stimulus). The physical unit of the turnover resistances is energy times time per unit volume. Each of these coefficients embeds the characteristic time related to the associated individual turnover mechanism.

Cell actions. The turnover resistances related to bone deposition and resorption are assumed to be related to cell concentrations. The higher the OB/OC concentration, the faster the rate of deposition/resorption of bone. Let [OB] and [OC] represent the concentrations of OB and OC, respectively. Thus, the turnover resistances read

$$d_{\mathsf{U}}^{\mathsf{OB}} = \frac{\bar{d}_{\mathsf{U}}^{\mathsf{OB}}}{[\mathsf{OB}]}, \tag{50}$$

$$d_{\mathsf{U}}^{\mathsf{OC}} = \frac{\bar{d}_{\mathsf{U}}^{\mathsf{OC}}}{[\mathsf{OC}]}, \tag{51}$$

$$d_{\mathsf{M}}^{\mathsf{OC}} = \frac{\bar{d}_{\mathsf{M}}^{\mathsf{OC}}}{[\mathsf{OC}]}. \tag{52}$$

The coefficients $\bar{d}_{\pi}^{\varpi} > 0$ are reference values of the renewing resistances that correspond to unit cell concentrations.

Several paracrine and autocrine signaling pathways occur in regulating the dynamics of OB and OC populations [38]. However, for the sake of simplicity, we leave aside here any mechanobiological argument and simply assume that OB and OC concentrations are proportional to that of OT. Moreover, we assume that OT concentration is proportional to the product between the volume fraction of bone matrix ($\phi_{\mathrm{bm}} = \phi_{\mathsf{U}} + \phi_{\mathsf{M}}$) and porosity ($\phi_{\mathsf{Por}}$). The rationale for this hypothesis is twofold: on the one hand, OT are embedded in the solid matrix of bone. On the other hand, cell metabolism requires exchanging water and other chemicals with the environment, that is prevented if the porosity drops below a critical value ($\phi_{\mathsf{Por}}^{\min}$). Therefore, the concentrations of OB and OC read

$$[\mathsf{OB}] = \beta^{\mathsf{OB}}(t)\, S_V, \tag{53}$$

$$[\mathsf{OC}] = \beta^{\mathsf{OC}}(t)\, S_V, \tag{54}$$

where $S_V = (\phi_{\mathsf{U}} + \phi_{\mathsf{M}}) \times (\phi_{\mathsf{Por}} - \phi_{\mathsf{Por}}^{\min})$ is a dimensionless parameter related to the specific surface of bone tissue (whose actual physical unit is the inverse of a length, see for instance the expression obtained in [39] based on the experimental measures of [40]). The time-dependent, positive coefficients $\beta^{\varpi} > 0$ modulate the concentration of cell populations $\varpi \in \{\mathsf{OB}, \mathsf{OC}\}$. If cell concentrations are measured as numbers of cells per unit volume, the physical unit of $\bar{d}_{\pi}^{\varpi}$ is energy times time and that of β^{ϖ} is the inverse of a volume. As the number of OC per unit volume is smaller than that of OB, it is expected that $\beta^{\mathsf{OC}} < \beta^{\mathsf{OB}}$.

Mineralization. It is assumed that mineralization becomes harder and harder as the volume fraction of unmineralized bone decreases. The rationale for this assumption is that U-bone first mineralizes in regions that are easily accessible to the chemicals involved in this reaction. As mineralization proceeds, the available U-bone is in regions that are increasingly remote for these chemicals, thus decreasing the likelihood for mineralization to take place even further. Similarly, demineralization is assumed to become harder and harder as the volume fraction of mineralized bone decreases. Combining these two assumptions, the following expression is proposed for the mineralization resistance:

$$d^{\chi} = \frac{\bar{d}^{\chi}}{\phi_{\mathsf{U}}\, \phi_{\mathsf{M}}}, \tag{55}$$

where $\bar{d}^{\chi} > 0$ is a reference value of the mineralization resistance.

Turnover stimuli. The turnover stimuli $\mathring{\lambda}_{\mathsf{U}}^{\mathsf{OB}}$, $\mathring{\lambda}_{\mathsf{U}}^{\mathsf{OC}}$, $\mathring{\lambda}_{\mathsf{M}}^{\mathsf{OC}}$, and $\Delta\mathring{\lambda}^{\chi}$ represent the actions that the biochemical environment exert on each individual mechanism of bone turnover. Their physical unit is energy per unit volume.

Cell actions. The outer stimuli $\overset{\circ}{\lambda}{}_{\mathsf{U}}^{\mathsf{OB}}$, $\overset{\circ}{\lambda}{}_{\mathsf{U}}^{\mathsf{OC}}$, and $\overset{\circ}{\lambda}{}_{\mathsf{M}}^{\mathsf{OC}}$ encode the external stimuli fostering bone deposition and resorption. Modeling these actions in detail is out of the scope of this paper. Here, we make very simple hypotheses relating these stimuli to the composition of the bone tissue, namely:

$$\overset{\circ}{\lambda}{}_{\mathsf{U}}^{\mathsf{OB}} = \alpha_{\mathsf{U}}^{\mathsf{OB}}(t)\, S_V, \tag{56}$$

$$\overset{\circ}{\lambda}{}_{\mathsf{U}}^{\mathsf{OC}} = \alpha_{\mathsf{U}}^{\mathsf{OC}}(t)\, \phi_{\mathsf{U}}\, (\phi_{\mathsf{Por}} - \phi_{\mathsf{Por}}^{\min}), \tag{57}$$

$$\overset{\circ}{\lambda}{}_{\mathsf{M}}^{\mathsf{OC}} = \alpha_{\mathsf{M}}^{\mathsf{OC}}(t)\, \phi_{\mathsf{M}}\, (\phi_{\mathsf{Por}} - \phi_{\mathsf{Por}}^{\min}). \tag{58}$$

Equation (56) relates the stimulus to the OB action to the availability of a solid substrate on which OB may lay down new bone and of a porosity allowing chemical exchanges. Equation (57) and Equation (58) relate the stimuli to the OC action to the availability of bone to be removed (U-bone and M-bone, respectively) and of a porosity allowing chemical exchanges. The time-dependent coefficients α_{π}^{ϖ} represent the unit stimuli and should comply with some physical constraints. On the one hand, OB lay down new bone, therefore the net stimulus $\overset{\mathsf{n}}{\lambda}{}_{\mathsf{U}}^{\mathsf{OB}} = \overset{\circ}{\lambda}{}_{\mathsf{U}}^{\mathsf{OB}} - \overset{\mathsf{i}}{\lambda}{}_{\mathsf{U}}^{\mathsf{OB}}$ is expected to be positive. On the other hand, OC remove bone, therefore the net stimuli $\overset{\mathsf{n}}{\lambda}{}_{\mathsf{U}}^{\mathsf{OC}} = \overset{\circ}{\lambda}{}_{\mathsf{U}}^{\mathsf{OC}} - \overset{\mathsf{i}}{\lambda}{}_{\mathsf{U}}^{\mathsf{OC}}$ and $\overset{\mathsf{n}}{\lambda}{}_{\mathsf{M}}^{\mathsf{OC}} = \overset{\circ}{\lambda}{}_{\mathsf{M}}^{\mathsf{OC}} - \overset{\mathsf{i}}{\lambda}{}_{\mathsf{M}}^{\mathsf{OC}}$ are expected to be negative. Note that the coefficients $\alpha_{\mathsf{U}}^{\mathsf{OC}}$ and $\alpha_{\mathsf{M}}^{\mathsf{OC}}$ may be different if the OC are more inclined to remove M-bone than U-bone.

Mineralization. The outer stimulus to mineralization $\Delta\overset{\circ}{\lambda}{}^{\chi}$ encodes the action of the chemical environment triggering the transition from the unmineralized to the mineralized state of bone solid matrix. It is introduced in Equation (34) as the difference between the outer stimuli fostering mineralization and demineralization. As mineralization ($\dot{\phi}_{\mathsf{U}}^{\mathsf{OB}} > 0$) is the natural process in physiological condition, this term should produce a positive net stimulus. However, the chemical equilibrium of the environment could also be shifted in order to foster demineralization ($\dot{\phi}_{\mathsf{U}}^{\mathsf{OB}} < 0$), e.g. lowering the pH of the interstitial fluid. In this case, $\Delta\overset{\circ}{\lambda}{}^{\chi}$ should produce a negative net stimulus. Note that, in particular, this term may change in time with respect to the calcium demands of the organism.

Evolution laws. Combining Equations (45-48), Equations (50-55), and Equations (56-54), the following set of nonlinear ordinary differential equations are obtained governing bone turnover:

$$\dot{\phi}_{\mathsf{U}}^{\mathsf{OB}} = \frac{[\mathsf{OB}]}{\bar{d}_{\mathsf{U}}^{\mathsf{OB}}} \left(\alpha_{\mathsf{U}}^{\mathsf{OB}}\, S_V - \overset{\psi}{\lambda}{}_{\mathsf{U}}^{\mathsf{mech}} - \overset{\psi}{\lambda}{}_{\mathsf{U}}^{\mathsf{chem}} \right), \tag{59}$$

$$\dot{\phi}_{\mathsf{U}}^{\mathsf{OC}} = \frac{[\mathsf{OC}]}{\bar{d}_{\mathsf{U}}^{\mathsf{OC}}} \left(\alpha_{\mathsf{U}}^{\mathsf{OC}}\, \phi_{\mathsf{U}}\, (\phi_{\mathsf{Por}} - \phi_{\mathsf{Por}}^{\min}) - \overset{\psi}{\lambda}{}_{\mathsf{U}}^{\mathsf{mech}} - \overset{\psi}{\lambda}{}_{\mathsf{U}}^{\mathsf{chem}} \right), \tag{60}$$

$$\dot{\phi}_{\mathsf{M}}^{\mathsf{OC}} = \frac{[\mathsf{OC}]}{\bar{d}_{\mathsf{M}}^{\mathsf{OC}}} \left(\alpha_{\mathsf{M}}^{\mathsf{OC}}\, \phi_{\mathsf{M}}\, (\phi_{\mathsf{Por}} - \phi_{\mathsf{Por}}^{\min}) - \overset{\psi}{\lambda}{}_{\mathsf{M}}^{\mathsf{mech}} - \overset{\psi}{\lambda}{}_{\mathsf{M}}^{\mathsf{chem}} \right), \tag{61}$$

$$\dot{\phi}_{\mathsf{M}}^{\chi} = \frac{\phi_{\mathsf{U}}\, \phi_{\mathsf{M}}}{\bar{d}^{\chi}} \left(\Delta\overset{\circ}{\lambda}{}^{\chi} - \Delta\overset{\psi}{\lambda}{}^{\mathsf{mech}} - \Delta\overset{\psi}{\lambda}{}^{\mathsf{chem}} \right), \tag{62}$$

where the expressions of $\overset{\psi}{\lambda}{}_{\mathsf{U}}^{\mathsf{mech}}$, $\overset{\psi}{\lambda}{}_{\mathsf{U}}^{\mathsf{chem}}$, $\overset{\psi}{\lambda}{}_{\mathsf{M}}^{\mathsf{mech}}$, $\overset{\psi}{\lambda}{}_{\mathsf{M}}^{\mathsf{chem}}$, $\Delta\overset{\psi}{\lambda}{}^{\mathsf{mech}}$, and $\Delta\overset{\psi}{\lambda}{}^{\mathsf{chem}}$ are given in Equations (30-31) and Equations (35-36) and those of [OB] and [OC] in Equations (53-54). Note that $\overset{\psi}{\lambda}{}_{\mathsf{U}}^{\mathsf{mech}}$, $\overset{\psi}{\lambda}{}_{\mathsf{M}}^{\mathsf{mech}}$, and $\Delta\overset{\psi}{\lambda}{}^{\mathsf{mech}}$ are equal to zero if the gross strain is null.

Equations (59-62) shall be solved by assigning initial conditions on the volume fractions of the U-bone and M-bone: $\phi_{\mathsf{U}}(t=0) = \phi_{\mathsf{U}}^0$ and $\phi_{\mathsf{M}}(t=0) = \phi_{\mathsf{M}}^0$. Once the individual turnover velocities are computed at a given time, the overall rates of U-bone and M-bone result from Equations (2-3), which allow updating the actual values of ϕ_{U} and ϕ_{M}. Moreover, at any time, the porosity is computed as $\phi_{\mathsf{Por}}(t) = 1 - \phi_{\mathsf{U}}(t) - \phi_{\mathsf{M}}(t)$.

Table 1. Reference values of the relevant model parameters grouped by category. Physical units: J, energy; T, time; L, length.

Parameter	Value
Resistances/reference values	$[J.T/L^3]$
$\bar{d}_{\mathrm{U}}^{\mathrm{OB}}$	0.25
$\bar{d}_{\mathrm{U}}^{\mathrm{OC}}$	0.15
$\bar{d}_{\mathrm{M}}^{\mathrm{OC}}$	0.15
$\bar{d}^{\chi}$	0.5
Resistances/cell concentration	$[1/L^3]$
β^{OB}	5
β^{OC}	0.5
Stimuli/cell activation	$[J]$
$\alpha_{\mathrm{U}}^{\mathrm{OB}}$	2
$\alpha_{\mathrm{U}}^{\mathrm{OC}}$	−1.5
$\alpha_{\mathrm{M}}^{\mathrm{OC}}$	−15
Stimuli/mineralization	$[J/L^3]$
$\Delta\mathring{\lambda}^{\chi}$	2
Inner actions	$[J/L^3]$
$\overset{\psi}{\lambda}_{\mathrm{U}}^{\mathrm{chem}}$	0
$\overset{\psi}{\lambda}_{\mathrm{M}}^{\mathrm{chem}}$	0
$\Delta\overset{\psi}{\lambda}^{\mathrm{chem}\dagger}$	0
Initial values	$[-]$
ϕ_{U}^{0}	1/3
ϕ_{M}^{0}	1/3
$\phi_{\mathrm{Por}}^{0}{}^{\ddagger}$	1/3
Porosity threshold	$[-]$
$\phi_{\mathrm{Por}}^{\mathrm{min}}$	0.01

†Computed as $\Delta\overset{\psi}{\lambda}^{\mathrm{chem}} = \overset{\psi}{\lambda}_{\mathrm{M}}^{\mathrm{chem}} - \overset{\psi}{\lambda}_{\mathrm{U}}^{\mathrm{chem}}$, see Equation (36).
‡Computed as $\phi_{\mathrm{Por}}^{0} = 1 - \phi_{\mathrm{U}}^{0} - \phi_{\mathrm{M}}^{0}$.

3. Results and discussion

Numerical simulations have been performed to investigate bone turnover in different situations. The simulated scenarios are oversimplified to highlight the descriptive capability of our model and are not intended to quantitatively reproduce experimental results or *in vivo* conditions.

In this section we focus only on the biochemical stimuli of bone turnover. Therefore, hereinafter we always assume that the gross strain is null ($\mathrm{E} = 0$) and that there is no rotary remodeling ($\dot{\mathrm{R}}\mathrm{R}^{\mathrm{T}} = 0$). The problem to be solved is represented by Equations (59-62) with the additional conditions: $\overset{\psi}{\lambda}_{\mathsf{U}}^{\mathsf{mech}} = \overset{\psi}{\lambda}_{\mathsf{M}}^{\mathsf{mech}} = \Delta\overset{\psi}{\lambda}^{\mathsf{mech}} = 0$. The bone turnover model has been implemented in Matlab [41]. (Code is available from the authors upon request.)

The values of the relevant model parameters are summarized in Table 2. Values reported in this table have been chosen for illustration purposes and calibrated so as to obtain sensible results while taking into account the expected relations and restrictions mentioned in the previous sections. Lacking information on the chemical potentials of the constituent phases of bone, the chemical inner actions were identically set to zero. Thus, the outer stimuli represent the net turnover stimuli. Moreover, the time scale of the simulations is arbitrary.

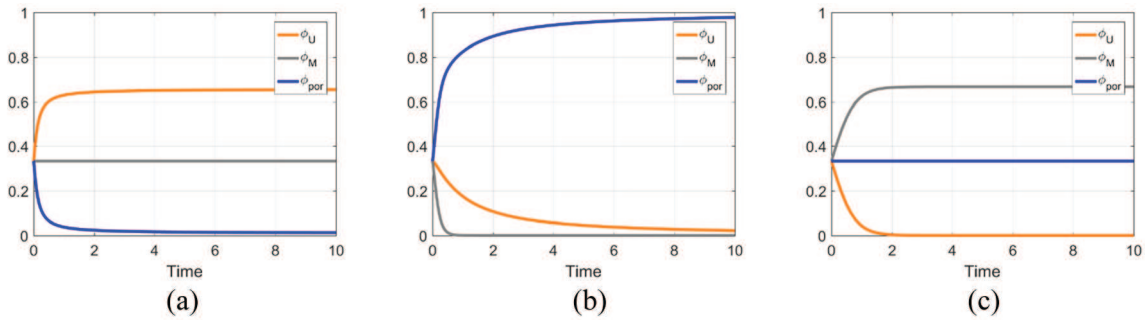

Figure 3. Evolution of bone volume fractions when only one turnover mechanism is activated: (a) OB activity; (b) OC activity; (c) mineralization. Time is in arbitrary units. U-bone: orange lines; M-bone: gray lines; porosity: blue lines.

3.1. Individual turnover mechanisms

As a first step, we checked whether the model can describe the physical scenarios depicted in Figure 2. To this aim, we studied the behavior of the model when only one turnover mechanism was activated and all the others were switched off. Results are depicted in Figure 3. Orange lines refer to the volume fractions of U-bone, gray lines to M-bone, and blue lines to porosity.

OB activity. In this scenario, OB activity is the only active turnover mechanism. Thus, Equations (60-62) were replaced with: $\dot{\phi}_{\mathsf{U}}^{\mathsf{OC}} = \dot{\phi}_{\mathsf{M}}^{\mathsf{OC}} = \dot{\phi}_{\mathsf{M}}^{\chi} = 0$. The evolution of the three bone phases is shown in Figure 3(a). It is apparent that the model describes the evolution depicted in Figure 2(b). Over time, OBs lay down new, unmineralized bone by progressively filling the available pore space. Therefore, the volume fraction of U-bone is observed to increase and that of porosity to decrease. Meanwhile, the volume fraction of M-bone does not change.

OC activity. In this scenario, OC activity is the only active turnover mechanism. Thus, Equations (59) and (62) were replaced with: $\dot{\phi}_{\mathsf{U}}^{\mathsf{OB}} = \dot{\phi}_{\mathsf{M}}^{\chi} = 0$. The evolution of the three bone phases is shown in Figure 3(b). It is apparent that the model describes the evolution depicted in Figure 2(c). Over time, OCs remove bone matrix and progressively enlarge the pore space. Therefore, the volume fraction of both M-bone and U-bone are observed to decrease and that of porosity to increase. Note that M-bone is removed faster than U-bone since OC are more inclined to remove old bone ($|\alpha_{\mathsf{M}}^{\mathsf{OC}}| > |\alpha_{\mathsf{U}}^{\mathsf{OC}}|$).

Mineralization. In this scenario, mineralization is the only active turnover mechanism. Thus, Equations (59-61) were replaced with: $\dot{\phi}_{\mathsf{U}}^{\mathsf{OB}} = \dot{\phi}_{\mathsf{U}}^{\mathsf{OC}} = \dot{\phi}_{\mathsf{M}}^{\mathsf{OC}} = 0$. The evolution of the three bone phases is shown in Figure 3(c). It is apparent that the model describes the evolution depicted in Figure 2(d). Over time, the unmineralized bone progressively turns into mineralized bone. Therefore, the volume fraction of U-bone is observed to decrease and that of M-bone to increase. Meanwhile, the porosity does not change.

3.2. Combined turnover mechanisms

When the three turnover mechanisms are activated simultaneously, a more complex behavior is observed. The evolution of the volume fractions of bone phases are depicted in Figure 4. After a transient phase, the volume fractions converge to stationary values independent of the initial bone composition. The scenarios simulated in Figure 4 correspond to three different initial conditions for the volume fractions of the bone phases: (a) identical values (as per Table 1), (b) highly mineralized bone ($\phi_{\mathsf{U}}^0 = 0.05$, $\phi_{\mathsf{M}}^0 = 0.9$, $\phi_{\mathsf{Por}}^0 = 0.05$), and (c) poorly mineralized bone ($\phi_{\mathsf{U}}^0 = 0.9$, $\phi_{\mathsf{M}}^0 = 0.05$, $\phi_{\mathsf{Por}}^0 = 0.05$). In the initial transient phase, the competition of the unbalanced turnover mechanisms results in fluctuations of the volume fractions that depend on the initial conditions. Afterward, whatever the initial conditions, the volume fractions smoothly converge toward their respective stationary values, namely: $\phi_{\mathsf{U}}^{\mathrm{st}} = 0.19$, $\phi_{\mathsf{M}}^{\mathrm{st}} = 0.67$, $\phi_{\mathsf{Por}}^{\mathrm{st}} = 0.14$.

It is worth noting that the final stationary values of the volume fractions correspond to a *dynamic equilibrium* where the competing effects of the different turnover mechanisms are balanced. The concept of *dynamic equilibrium* is borrowed from the chemistry and physics of multi-phase systems and does not involve any inertia.

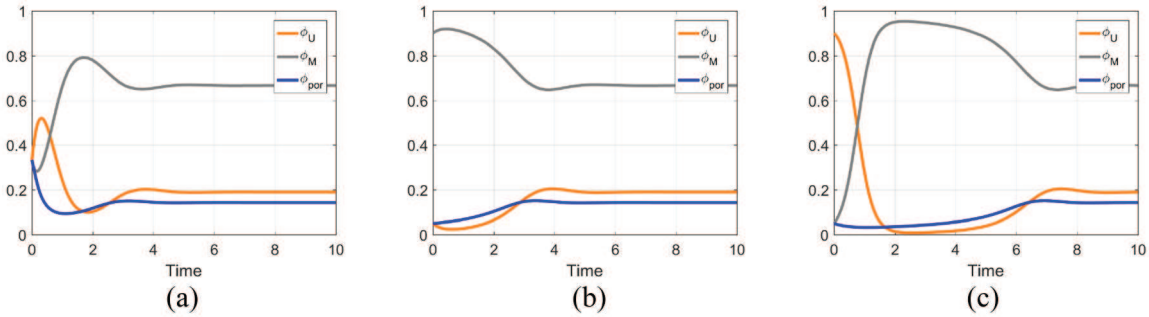

Figure 4. Evolutions of bone volume fractions when all the turnover mechanisms are activated. Three different initial conditions are considered: (a) identical values for all the volume fractions (as per Table 1), (b) highly mineralized bone ($\phi_{\mathrm{U}}^0 = 0.05$, $\phi_{\mathrm{M}}^0 = 0.95$, $\phi_{\mathrm{Por}}^0 = 0.05$), and (c) poorly mineralized bone ($\phi_{\mathrm{U}}^0 = 0.95$, $\phi_{\mathrm{M}}^0 = 0.05$, $\phi_{\mathrm{Por}}^0 = 0.05$). U-bone: orange lines; M-bone: gray lines; Porosity: blue lines.

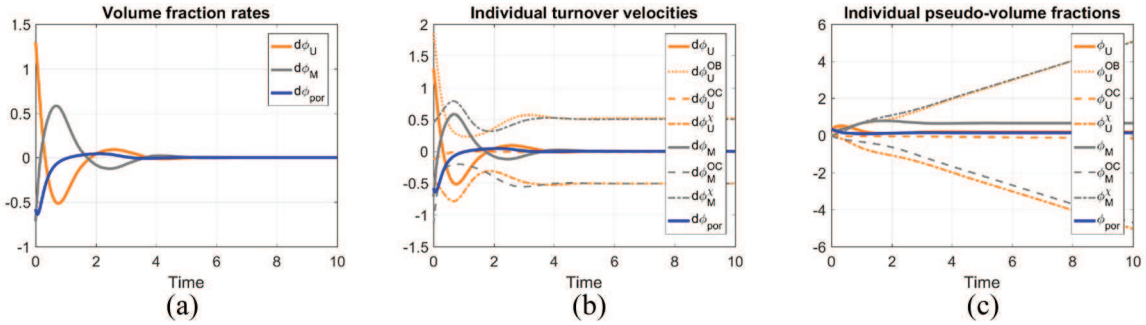

Figure 5. Evolutions of (a) overall turnover velocities ($\mathrm{d}\phi_\pi \equiv \dot{\phi}_\pi$), (b) individual turnover velocities ($\mathrm{d}\phi_\pi^\varpi \equiv \dot{\phi}_\pi^\varpi$), and (c) corresponding pseudo-volume fractions for the scenario in Figure 4(a). Orange lines refer to U-bone, gray lines to M-bone, and blue lines to porosity. Dotted lines refer to OB activity, dashed lines to OC activity, dash-dotted lines to mineralization, and solid lines to the overall effects.

This is illustrated in Figure 5 for the scenario in Figure 4(a). As the system approaches its stationary state, the overall turnover velocities (Figure 5(a)) go to zero and therefore the volume fractions reach a stationary state. However, the individual turnover mechanisms are still active: the individual turnover velocities (Figure 5(b)) reach a stationary, non-zero value and, accordingly, the corresponding pseudo-volume fractions (Figure 5(c)) evolve linearly in time. Looking at Figure 5(b), it can be observed that, at any time, the volume of U-bone laid down by OBs at the rate $\dot{\phi}_{\mathrm{U}}^{\mathrm{OB}}$ (orange, dotted line) is partially removed by OC at the rate $\dot{\phi}_{\mathrm{U}}^{\mathrm{OC}}$ (orange, dashed line) and partially undergoes mineralization turning into M-bone at the rate $\dot{\phi}_{\mathrm{U}}^{\chi}$ (orange, dash-dotted line). The net effect of these phenomena produces the visible evolution of the U-bone depicted by orange, solid lines in Figures 5(a)–(c). At the equilibrium, the rate of production of U-bone ($\dot{\phi}_{\mathrm{U}}^{\mathrm{OB}}$) is balanced with the rate of resorption ($\dot{\phi}_{\mathrm{U}}^{\mathrm{OC}}$) and mineralization ($\dot{\phi}_{\mathrm{U}}^{\chi}$), leading to a null net production of U-bone ($\dot{\phi}_{\mathrm{U}}$). Similarly, the M-bone produced by mineralization of U-bone at the rate $\dot{\phi}_{\mathrm{M}}^{\chi}$ (gray, dash-dotted line) is removed by the OC at the rate $\dot{\phi}_{\mathrm{M}}^{\mathrm{OC}}$, leading to a net effect depicted by the gray, solid lines in Figure 5(a)–(c). At the equilibrium, the rate of production of M-bone by mineralization ($\dot{\phi}_{\mathrm{M}}^{\chi}$) is balanced with the rate of resorption by the OC ($\dot{\phi}_{\mathrm{M}}^{\mathrm{OC}}$), leading to a null net production of M-bone ($\dot{\phi}_{\mathrm{M}}$). Of course, when both volume fractions of U-bone and M-bone stabilize, the porosity does not evolve any more (blue, solid lines in Figure 5(a)–(c)).

3.3. Perturbed turnover mechanisms

In this section we aim at investigating the effects of perturbations of the turnover mechanisms. Thus, we performed different simulations starting from the stationary state of the system and modifying the strength of one turnover mechanisms at once. To this aim, we multiplied the right-hand side of either of Equations (59-62) by a coefficient $a \in [0.75, 1.25]$, which corresponds to perturbing one net turnover stimulus at a time of $\pm 25\%$.

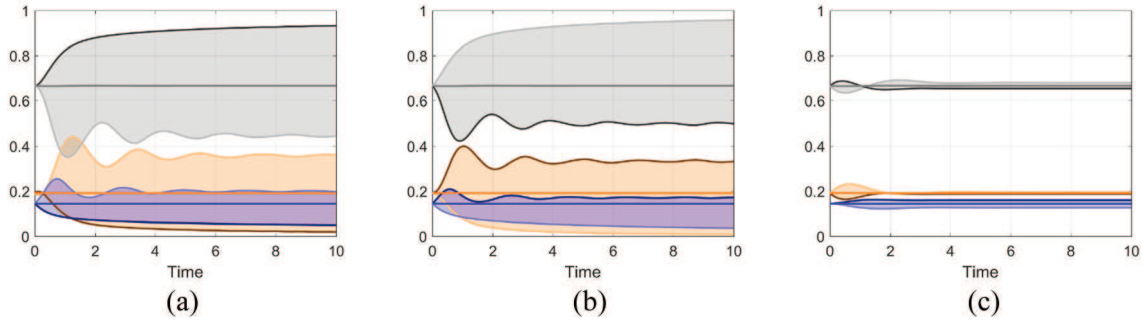

Figure 6. Evolution of bone volume fractions from the stationary state when perturbing one turnover mechanism at once: (a) osteoblast activity; (b) osteoclast activity; (c) mineralization. U-bone: orange lines; M-bone: gray lines; porosity: blue lines.

Results are shown in Figure 6. Shaded areas depict the trajectories followed by the system when varying the parameter a. Lower and upper bounds are shown by lines in light and dark colors, respectively. The trajectories corresponding to the reference scenarios ($a = 1$) are also shown (lines in pure colors).

OB activity. In this scenario, OB activity is the only perturbed turnover mechanism. Simulations were run by perturbing Equation (59) and results are shown in Figure 6(a). It is apparent that OB activity has a strong effect on the evolution of the system. As expected, as the OB activity increases, the porosity decreases. On the other hand, the volume fraction of M-bone increases and that of U-bone decreases. This results from the simple law adopted for scaling the cell populations with the bone composition, namely with respect to the porosity. Let us consider the case where OB activity is strengthened. At the very beginning of the turnover process, the increased OB activity leads to a reduction of porosity. As the porosity decreases, the OB concentration decreases as well (see Equation (53)) and, quite soon, the right-hand side of Equation (59) drops below its reference value. Therefore, except for the very initial phase where the volume fraction of U-bone actually increases, the rate of production of U-bone is strongly reduced and cannot compensate for the mineralization process. Thus, overall, the volume fraction of M-bone is observed to increase at the expense of the available U-bone.

OC activity. In this scenario, OC activity is the only perturbed turnover mechanism. Simulations were run by perturbing Equations (60-61) and results are shown in Figure 6(b). Similarly to the previous case, perturbing the OC activity has a strong effect on the evolution of the system. Increasing the OC activity leads, on the one hand, to an increase of porosity and U-bone and, on the other hand, to a decrease of M-bone. Moreover, the system shows fluctuation of increasing amplitude and seems to saturate toward a value of porosity close to 0.2. This behavior is related to the complex interaction between OC and OB in this regime of cell activities. The saturation value of the porosity is not an upper bound but rather corresponds to a singular state of the system after which the latter switches in a different regime. Actually, enhancing even more the OC activity (e.g., $a = 10$), the action of OC prevails on that of OB and the porosity smoothly increases up to 1. (Data not shown.)

Mineralization. In this scenario, mineralization is the only perturbed turnover mechanism. Simulations were run by perturbing Equation (62) and results are shown in Figure 6(c). A perturbation of the mineralization mechanism has little effect on the system. The main effect is to change the transient dynamics of the system, whereas the limit state is almost unchanged with respect to the reference case. Increasing the mineralization stimulus, the volume fraction of M-bone is observed to initially increase and then decrease to a limit value slightly smaller than in the reference case. Actually, the initial increase of M-bone has a positive effect on the OC stimulus ($\mathring{\lambda}_{\mathsf{U}}^{\mathsf{OC}}$ which depends on ϕ_{M}, see Equation (58)) and little effect on the OB stimulus (that depends on S_V and therefore on $\phi_{\mathsf{U}} + \phi_{\mathsf{M}}$, see Equation (56)). In turn, increased OC activity leads to an increase of porosity and a decrease of M-bone.

4. Conclusion

We have proposed a new model to describe the remodeling and turnover of bone tissue. The model is set in the framework of generalized continuum mechanics following the pioneering ideas of [28, 30]. While keeping a macroscopic description of bone, this approach allows the description of the evolution of its microstructure to be considered. The kinematic description of bone material points is enriched with additional parameters describing the average organization of bone microstructure. After setting up the general model, the focus was set on the biochemical mechanisms of bone turnover, i.e., the evolution of bone composition, and toy models have been proposed for the turnover resistances and stimuli following physically sound hypotheses. Thus, bone turnover is described by a set of nonlinear ordinary differential equations describing the individual mechanisms of turnover, namely OB activity, OC activity, and mineralization (see Equations (59-62)). The net bone turnover results from the dynamic equilibrium of these competitive mechanisms. It is worth noting that the model equations can be combined in order to provide the net gain/loss of bone mass which reads

$$\phi_{\mathrm{bm}} = k_{\mathrm{for}}\,[\mathsf{OB}] - k_{\mathrm{res}}\,[\mathsf{OC}], \tag{63}$$

where ϕ_{bm} is the volume fraction of bone matrix and k_{for} and k_{res} are (time-dependent) bone-formation and bone-resorption coefficients, respectively. This expression is similar to that obtained in [42]. In that paper, the authors used a complex mechanobiological model to link the evolution of bone to the bone cell concentrations. By contrast, k_{for} and k_{res} were considered as time-invariant properties. One of the main limitations of our model is the lack of mechanobiological feedback. Indeed, we related the cell concentrations and the expressions of k_{for} and k_{res} to the composition of bone tissue. Mechanobiological models linking bone remodeling with the mechanical state of the material (strain, stress, energy density, etc.) and accounting for the biochemical crosstalk between the different bone cell populations have greater potential in describing the actual dynamics of bone remodeling [42–48]. Indeed, although our model is capable to describe the main features of bone turnover, in some cases we observed non intuitive results that did not fully capture the balance between cells turnover and mineralization. This is likely due to the toy models used for the turnover resistances and stimuli–see discussion in the section focusing on perturbed turnover mechanisms. The goal of this paper being the development of the general bone turnover model, as a first approximation we were required to make simplifying assumptions. We will improve our constitutive theory in future work, including the expressions of the mechanical and chemical energy densities. In particular, we aim at replacing our phenomenological constitutive assumptions on the turnover resistances and stimuli with physically-sound, mechanobiological models of cell dynamics [38, 49, 50] and non-local models of biological stimuli [51, 52].

Our numerical results provided a qualitative description of the model behavior that allowed understanding its current descriptive capability and its limitations. In particular, we do not pretend nor expect to obtain too realistic results. Thus, calibration of the model parameters was not the major aim of this paper. Nevertheless, this is another critical point which definitely requires further attention and that will be addressed in future work. Using calibrated models of cell dynamics will likely reduce the number of model parameters and simplify the calibration process.

Finally, we stress that, although in this paper we focused on the biochemical mechanisms of bone turnover, our model does account for the effects of bone remodeling on the mechanical behavior of bone material. The chemomechanical coupling is set at the constitutive level, namely in the functional dependence of the strain energy on bone composition, see Equation (14). Similarly to [53, 54], this makes bone composition affect the elastic response of bone. This coupling is not relevant as long as the gross deformation is null, as in the numerical simulations of this paper, but it becomes a main issue in a more general setting. Investigation of the chemomechanical coupling will be done in future work.

Funding

The author(s) disclosed receipt of the following financial support for the research, authorship, and/or publication of this article: This work has received funding from the European Research Council (ERC) under the European Union's Horizon 2020 research and innovation program (Grant Agreement No. 682001, project ERC Consolidator Grant 2015 BoneImplant).

References

[1] Bonewald, LF, and Johnson, ML. Osteocytes, mechanosensing and Wnt signaling. *Bone* 2008; 42(4): 606–615.

[2] Jee, WSS. Integrated bone tissue physiology: Anatomy and physiology. In: *Bone Mechanics Handbook*. Boca Raton, FL: CRC Press, 2001.

[3] Fratzl, P, Gupta, HS, Paschalis, EP, et al. Structure and mechanical quality of the collagen-mineral nano-composite in bone. *J Mater Chem* 2004; 14(14): 2115–2123.
[4] Berridge, MJ, Bootman, MD, and Lipp, P. Calcium—a life and death signal. *Nature* 1998; 395(6703): 645–648.
[5] Confavreux, CB. Bone: From a reservoir of minerals to a regulator of energy metabolism. *Kidney Int* 2011; 79(Suppl. 121): S14–S19.
[6] Penido, MGMG, and Alon, US. Phosphate homeostasis and its role in bone health. *Ped Nephrol* 2012; 27(11): 2039–2048.
[7] Culmann, K. *Die graphische Statik*. Zurich: Meyer & Zeller (A. Reimann), 1866.
[8] von Meyer, GH. Die Architektur der Spongiosa. (Zehnter Beitrag zur Mechanik des menschlichen Knochgerüstes). *Arch Anat Physiol wissensch Med* 1867; 6: 615–628.
[9] Wolff, J. Ueber die innere Architectur der Knochen und ihre Bedeutung für die Frage vom Knochenwachsthum. *Arch Pathol Anat Physiol Klin Med* 1870; 50(3): 389–450.
[10] Roux, W. *Der Kampf der Teile des Organismus*. Leipzig: Engelmann, 1881.
[11] Cowin, SC, and Hegedus, DH. Bone remodeling I: theory of adaptive elasticity. *J Elasticity* 1976; 6(3).
[12] Cowin, SC. Mechanical modeling of the stress adaptation process in bone. *Calcif Tissue Int* 1984; 36(Suppl. 1): S98–S103.
[13] Frost, HM. Bone "mass" and the "mechanostat": A proposal. *Anatom Record* 1987; 219(1): 1–9.
[14] Frost, HM. Perspectives: A proposed general model of the "mechanostat" (suggestions from a new skeletal-biologic paradigm). *Anatom Record* 1996; 244(2): 139–147.
[15] Jacobs, CR, Simo, JC, Beaupré, GS, et al. Adaptive bone remodeling incorporating simultaneous density and anisotropy considerations. *J Biomech* 1997; 30(6): 603–613.
[16] Luo, JH, and Gea, HC. Optimal orientation of orthotropic materials using an energy based method. *Struct Optimiz* 1998; 15(3–4): 230–236.
[17] Luo, ZP, and An, KN. A theoretical model to predict distribution of the fabric tensor and apparent density in cancellous bone. *J Math Biol* 1998; 36(6): 557–568.
[18] Fernandes, P, Rodrigues, H, and Jacobs, CR. A model of bone adaptation using a global optimisation criterion based on the trajectorial theory of Wolff. *Comput Meth Biomech Biomed Eng* 1999; 2(2): 125–138.
[19] Miller, Z, Fuchs, MB, and Arcan, M. Trabecular bone adaptation with an orthotropic material model. *J Biomech* 2002; 35(2): 247–256.
[20] Shang, Y, Peng, L, and Bai, J. A three-dimensional orthotropic adaptation algorithm for femur remodeling. In: Magjarevic R and Nagel JH (eds.) *World Congress on Medical Physics and Biomedical Engineering 2006*. Berlin: Springer, 2006, pp. 3038–3040.
[21] Geraldes, DM, and Phillips, ATM. A comparative study of orthotropic and isotropic bone adaptation in the femur. *Int J Numer Meth Biomed Eng* 2014; 30(9): 873–889.
[22] Geraldes, DM, Modenese, L, and Phillips, AT. Consideration of multiple load cases is critical in modelling orthotropic bone adaptation in the femur. *Biomech Mod Mechanobiol* 2016; 15(5): 1029–1042.
[23] Doblaré, M, and García, JM. Application of an anisotropic bone-remodelling model based on a damage-repair theory to the analysis of the proximal femur before and after total hip replacement. *J Biomech* 2001; 34(9): 1157–1170.
[24] Doblaré, M, and García, JM. Anisotropic bone remodelling model based on a continuum damage-repair theory. *J Biomech* 2002; 35(1): 1–17.
[25] Martínez-Reina, J, García-Aznar, JM, Domínguez, J, et al. On the role of bone damage in calcium homeostasis. *J Theoret Biol* 2008; 254(3): 704–712.
[26] Ramtani, S, and Zidi, M. Damaged-bone remodeling theory: Thermodynamical approach. *Mech Res Commun* 1999; 26(6): 701–708.
[27] Goda, I, Ganghoffer, JF, and Maurice, G. Combined bone internal and external remodeling based on Eshelby stress. *Int J Solids Struct* 2016; 94–95: 138–157.
[28] DiCarlo, A, and Quiligotti, S. Growth and balance. *Mech Res Commun* 2002; 29(6): 449–456.
[29] DiCarlo, A, Sansalone, V, Tatone, A, et al. Growth and remodelling of intracranial saccular aneurysms. In *Proceedings of the COMSOL Conference*, Milan, 2009.
[30] DiCarlo, A, Naili, S, and Quiligotti, S. Sur le remodelage des tissus osseux anisotropes. *C R Mécanique* 2006; 334(11): 651–661.
[31] Germain, P. The method of virtual power in continuum mechanics. Part 2: Microstructure. *SIAM J Appl Math* 1973; 25(3): 556–575.
[32] Capriz, G. *Continua With Microstructure* (*Springer Tracts in Natural Philosophy*, Vol. 37). Berlin: Springer, 1989.
[33] Sansalone, V, Naili, S, and Di Carlo, A. On the rotary remodelling equilibrium of bone. *Comput Meth Biomech Biomed Eng* 2011; 14(Suppl. 1): 203–204.
[34] Martin, M, Pivonka, P, Haiat, G, et al. Bone orthotropic remodeling as a thermodynamically-driven evolution. *J Mech Med Biol* 2020; 20(4): 1950084.
[35] Pivonka, P, Buenzli, P, and Dunstan, C. A systems approach to understanding bone cell interactions in health and disease. In: *Cell Interaction*. InTech, 2012.
[36] Fratzl, P, Fratzl-Zelman, N, and Klaushofer, K. Collagen packing and mineralization. An x-ray scattering investigation of turkey leg tendon. *Biophys J* 1993; 64(1): 260–266.
[37] Podio-Guidugli, P. A primer in elasticity. *J Elasticity* 2000; 58: 1–104.

[38] Martin, M, Sansalone, V, Cooper, DML, et al. Mechanobiological osteocyte feedback drives mechanostat regulation of bone in a multiscale computational model. *Biomech Mod Mechanobiol* 2019; 18(5): 1475–1496.
[39] Pivonka, P, Buenzli, PR, Scheiner, S, et al. The influence of bone surface availability in bone remodelling - A mathematical model including coupled geometrical and biomechanical regulations of bone cells. *Eng Struct* 2013; DOI: 10.1016/j.engstruct.2012.09.006.
[40] Martin, RB. Porosity and specific surface of bone. *Crit Rev Biomed Eng* 1984; 10(3): 179–222.
[41] Matlab. *MATLAB® (R2017b)*. Natick, MA: The Mathworks, Inc., 2017.
[42] Scheiner, S, Pivonka, P, and Hellmich, C. Coupling systems biology with multiscale mechanics, for computer simulations of bone remodeling. *Comput Meth Appl Mech Eng* 2013; 254: 181–196.
[43] Lekszycki, T, and dell'Isola, F. A mixture model with evolving mass densities for describing synthesis and resorption phenomena in bones reconstructed with bioâŁłresorbable materials. *ZAMM* 2012; 92(6): 426–444.
[44] Hambli, R. Connecting mechanics and bone cell activities in the bone remodeling process: An integrated finite element modeling. *Front Bioeng Biotechnol* 2014; 2: 1–12.
[45] Scheiner, S, Pivonka, P, and Hellmich, C. Poromicromechanics reveals that physiological bone strains induce osteocyte-stimulating lacunar pressure. *Biomech Mod Mechanobiol* 2016; 15: 9–28.
[46] George, D, Allena, R, and Rémond, Y. A multiphysics stimulus for continuum mechanics bone remodeling. *Math Mech Complex Syst* 2018; 6(4): 307–319.
[47] George, D, Allena, R, and Rémond, Y. Integrating molecular and cellular kinetics into a coupled continuum mechanobiological stimulus for bone reconstruction. *Continuum Mech Thermodyn* 2019; 31(3): 725–740.
[48] Ganghoffer, J, Rahouadj, R, Boisse, J, et al. A phase field approach for bone remodeling based on a second-gradient model. *Mech Res Commun* 2019; 96: 37–44.
[49] Komarova, SV, Smith, RJ, Dixon, SJ, et al. Mathematical model predicts a critical role for osteoclast autocrine regulation in the control of bone remodeling. *Bone* 2003; DOI: 10.1016/S8756-3282(03)00157-1.
[50] Martin, M, Sansalone, V, Cooper, DML, et al. Assessment of romosozumab efficacy in the treatment of post-menopausal osteoporosis: Results from a mechanistic PK–PD mechanostat model of bone remodeling. *Bone* 2020; DOI: 10.1016/j.bone.2020.115223.
[51] Prendergast, P, and Taylor, D. Prediction of bone adaptation using damage accumulation. *J Biomech* 1994; 27(8): 1067–1076.
[52] Giorgio, I, dell'Isola, F, Andreaus, U, et al. On mechanically driven biological stimulus for bone remodeling as a diffusive phenomenon. *Biomech Mod Mechanobiol* 2019; 18: 1639–1663.
[53] Madeo, A, dell'Isola, F, and Darve, F. A continuum model for deformable, second gradient porous media partially saturated with compressible fluids. *J Mech Phys Solids* 2013; 61(11): 2196–2211.
[54] Giorgio, I, Andreaus, U, Scerrato, D, et al. A visco-poroelastic model of functional adaptation in bones reconstructed with bio-resorbable materials. *Biomech Mod Mechanobiol* 2016; 15(5): 1325–1343.